3rd European supercritical CO2 Conference
September 19-20, 2019, Paris, France

2019-sCO2.eu-110

DIRECT NUMERICAL SIMULATION OF FLOW AND HEAT TRANSFER WITHIN CHANNELS OF A SUPERCRITICAL CO_2 COOLER

Eckart Laurien*
Institute of Nuclear Technology and Energy Systems,
University of Stuttgart
Stuttgart, Germany
Email: Laurien@ike.uni-stuttgart.de

Sandeep Pandey
Institute of Nuclear Technology and Energy Systems,
University of Stuttgart
Stuttgart, Germany
Email: Pandey@ike.uni-stuttgart.de

ABSTRACT

The flow and heat transfer of supercritical CO_2 within representative channels of the cooler (condenser) of a proposed Brayton Cycle is investigated using Direct Numerical Simulation (DNS). The DNS method is based on the temporal and spatial integration of the fundamental conservation equations of motion and energy, the Navier Stokes Equations. Unlike other methods the DNS does not require a turbulence model, because all scales of the turbulence structures are numerically resolved on a very fine mech. The method is limited to low Reynolds numbers and is therefore performed only for a low mass flux density of 53.87 kg/m^{2}s. It requires the use of a High-Performance Computer Cray-XC 40. We have performed various DNS's of cooled circular pipes with a diameter of 2 mm and a length up to 60 diameters at 80 bars. The considered bulk temperature range between 69°C and 32°C is equivalent to the operational range of the cooler of the reference power cycle. The DNS wall-temperature data for two cases with different wall heat fluxes are smoothed and fitted with 3rd-order polynomials to constitute a practical prediction method for the wall heat flux at any given wall temperature based on interpolation. Under the assumption of a wall temperature of 25°C our results for the cooling wall heat flux are compared to existing empirical Nusselt correlations in order to demonstrate the differences of the various prediction methods. An attempt is made to scale our results to higher mass fluxes up to 2000 kg/m^{2}s and the influence of buoyancy on this scaling method is discussed. Finally, the minimum required length of the cooler at a given wall temperature of 25°C is estimated using both the existing correlations as well as the present DNS-based prediction method. It is found, that predictions using these methods differ by up to a factor of two! None of the existing correlation agrees completely with our DNS results but a recommendation about the best correlation for future cooler design is given.

1 INTRODUCTION

1.1 MOTIVATION

Various efficient recuperative Brayton Cycles using supercritical carbon dioxide (sCO_2) as working fluid have been proposed by Dostal et al. [1] . Here, we use the version denoted as 'advanced design', in which the low-pressure part is at 7.7 MPa, which is only slightly above the critical pressure of 7.38 MPa. The cooler operates within a temperature range between 68.9°C (inlet) and 32°C (outlet) corresponding to an enthalpy-range between approximately 480 kJ/kg (inlet) and 300 kJ/kg (outlet). Under these conditions, the heat transfer within the individual channels of the cooler is difficult to predict and large uncertainties may arise. However, an accurate prediction of flow and heat transfer is important for the design and off-design characteristics of the cooler, because its outlet temperature influences directly the subsequent compressor.

1.2 LITERATURE STATE

In this enthalpy range the fluid properties T (temperature), ρ (density), c_p (specific heat capacity), and λ (heat conductivity) of sCO_2 undergo significant changes, **figs. 1-4** [2]

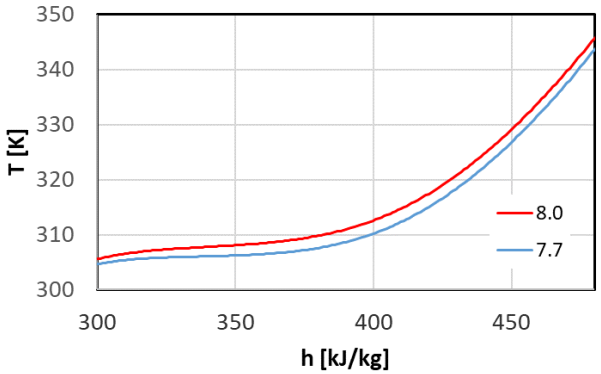

Figure 1: Temperature of sCO_2 vs. the enthalpy at two pressures in MPa.

* corresponding author

DOI: 10.17185/duepublico/48873

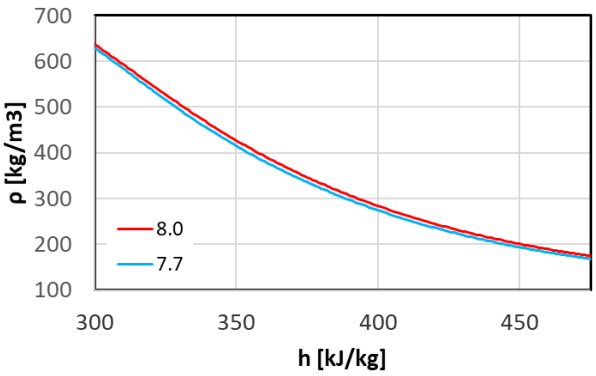

Figure 2: Same as figure 1 for the density.

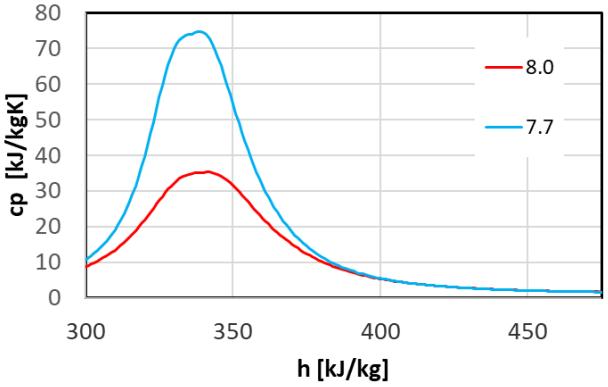

Figure 3: Same as figure 1 for the specific heat capacity.

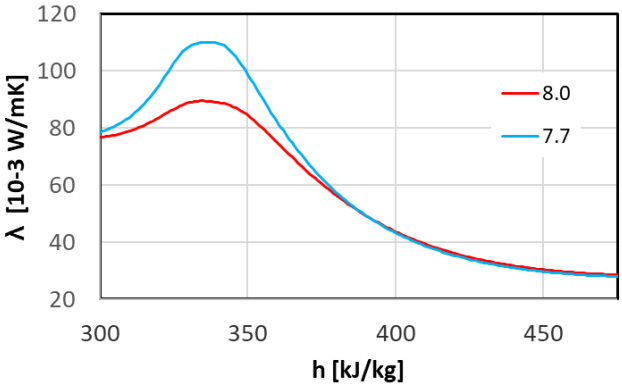

Figure 4: Same as figure 1 for the heat conductivity.

Due to the density increase the flow within the cooler channels of a compact heat exchanger experiences a drastical deceleration along the flow direction, which is from right to left in all figures throughout this paper. The turbulent heat transfer under these conditions is typically estimated or predicted by experimentally derived Nusselt correlations, which take the variable properties of sCO_2 but no buoyancy into account, see [3]. It is well known that significant deviations between the results of various correlations occur [4] , leaving uncertainty about their accuracy and validity during design. However, with the Direct Numerical Simulation (DNS) a new powerful investigation method of turbulent flows has recently become available to investigate and predict the turbulent heat transfer of sCO_2 [5-8]. It is based on the temporal and spacial numerical integration of the fundamental three-dimensional conservation equations of mass, momentum and energy, known as the Navier Stokes Equations. Unlike other numerical simulation methods the DNS does not require a turbulence model, because even the smallest scales of the turbulence structures are numerically resolved on a very fine mesh. This method is able to provide useful new information about the unstedy, turbulent velocity and temperature behaviour in a turbulent supercritical flow. Furthermore, it provides physically-based insight into the behavior of any flow quantity, which may be important in the design process.

1.2 AIM OF THIS WORK

In the present paper Direct Numerical Simulation is used to investigate the physical behaviour of flow turbulence in channels with a cirtcular cross section under the cooler conditions of the present cycle. A practical interpolation method to predict the wall temparature for any given wall heat flux, or vice versa, is derived from our simulation. Its results are compared to empirical heat-transfer correlations. Thus, we aim to provide guidelines about the capabilities and uncertainties of existing heat transfer correlations for practical cooler design. Finally, the calculation of the minimum required lengh of the cooler under given wall-temperature conditions is taken as an example to demonstrate the uncertainties. A recommendation about correlations, which are feasible for further calculations, is given.

2 SIMULATION MODEL

Direct Numerical Simulation (DNS) is based on the numerical integration of the fundamental conservation equations of mass, momentum and energy (Navier-Stokes Equations, NSE) within a three-dimensional integration domain, representing the flow field. Due to the absence of a turbulence model, a turbulent flow can only be simulated if all turbulent length and time scales, i.e. the motion and development of both the large and the small turbulent eddies, are numerically resolved. This leads to fine numerical grids, here 14.7 million cells, and small timesteps of the simulation. From the unsteady simulation results, many interesting local flow quantities can be derived by 3D visualization and statistical postprocessing. We have employed the low Mach number Navier-Stokes equations, in which it is assumed that during the heat transfer at supercritical pressure, the compressibility effects due to acoustic interactions and pressure changes can be decoupled from thermal interactions.

In eq. (1) the time is t, the quantities x_i and u_i ($i,j=1,2,3$) are Cartesian coordinates and velocity components. As the properties, we have the viscosity $\mu(h)$, the density $\rho(h)$, and the thermal conductvity $\lambda(h)$. The local pressure is p, and the temperature $T(h)$, where h the specific enthalpy. The unit vector in axial direction e_{ax} can be 1 (upward flow), -1 (downward flow) or zero (no gravity), with g = 9.81 kg/m^2. δij is the Kronecker operator (*1* for $i=j$ or *0* for $i\neq j$). The system represents the local,

DOI: 10.17185/duepublico/48873

instantaneous conservation of mass, momentum and enthalpy of a turbulent flow

$$\frac{\partial \rho}{\partial t}+\frac{\partial\left(\rho u_j\right)}{\partial x_j}=0$$

$$\frac{\partial\left(\rho u_i\right)}{\partial t}+\frac{\partial\left(\rho u_i u_j\right)}{\partial x_j}= \tag{1}$$

$$\rho g\, e_{ax}-\frac{\partial p}{\partial x_i}+\frac{\partial}{\partial x_j}\mu\left(\frac{\partial u_i}{\partial x_j}+\frac{\partial u_j}{\partial x_i}-\frac{2}{3}\delta_{ij}\frac{\partial u_k}{\partial x_k}\right)$$

$$\frac{\partial(\rho h)}{\partial t}+\frac{\partial\left(\rho u_j h\right)}{\partial x_j}=\frac{\partial}{\partial x_j}\lambda\frac{\partial T}{\partial x_j}$$

The integration domain of our simulation model [9-10] is shown in **fig. 5**. It covers the region within a straight circular pipe with diameter $D=2$ *mm* and length L up to $60D$. In this domain, the above NSE are integrated by the finite-volume method.

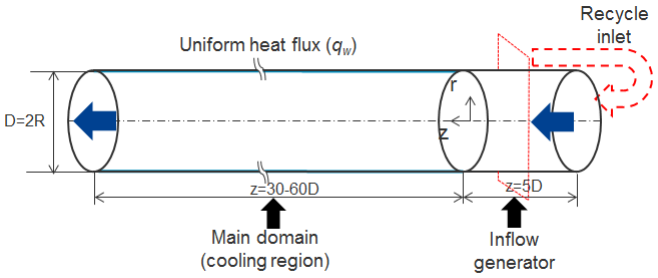

Figure 5: Integration domain and boundary conditions.

As boundary conditions, a flow of given mass flow rate G is imposed by adjusted pressure values at the flow inlet (right in **fig. 5**) and outlet (left). The pressure at the inlet is 8 MPa. The inlet temperature T_{in} is prescribed to fit cooler-relevant conditions. The wall is cooled with a given heat-flux density q_w, except within a short adiabatic inlet section to allow for the development of turbulence before cooling is applied. The fluid properties are determined locally as functions of the enthalpy h. As part of the NSE, gravity is defined such that the flow is either upward or downward, denoted as 'mixed convection'. An artificial case without gravity is denoted as 'forced'. Turbulence develops under the influence of shear, deceleration, and buoyancy. The processed data from these simulations are available online[1].

3.1 PHYSICAL INTERPRETATION OF RESULTS

We have investigated the physical aspects of turbulence development under wall-cooling conditions by an analysis of the small-scale flow structures [11-12]. The simulation results show the impaired heat transfer during downward flow and an enhanced heat transfer during the upward flow, contrary to the heating of sCO_2 [5-8]. In the downward flow, heat transfer is deteriorated initially but soon enough a heat transfer recovery was observed (see **fig. 6**). The main reason for deteriorated heat transfer is the reduction in turbulence until $z=20D$ in the downward flow due to the adverse effects of the body force as a result of buoyancy as evident from **fig. 7**, which shows the instantaneous mass-flux streaks in the near wall region. The turbulent streaks were visualized by the deviation from their temporal average. The formation and breakdown of streaks can be observed in the inlet section ($z=0$-$5D$).

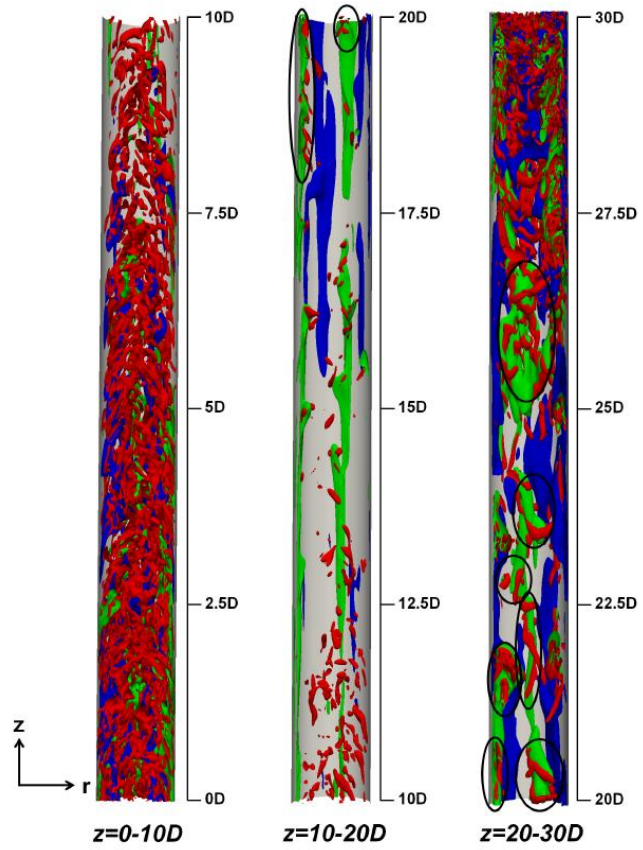

Figure 6: Iso-surfaces of streaks and vortex structure along the pipe for downward flow; blue: low speed streaks; green: high speed streaks; red: $\lambda 2$ vortex criterion.

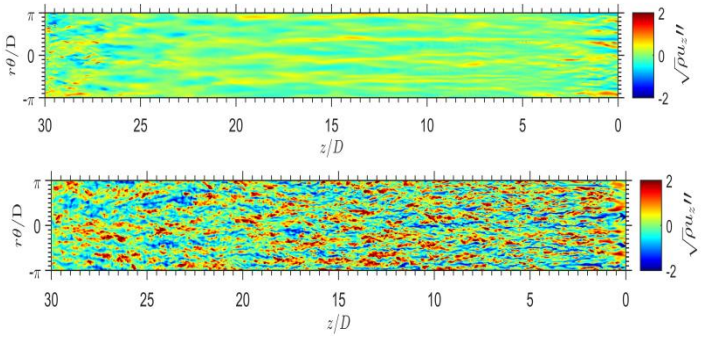

Figure 7: Visualization of the instantaneous streaks for downward (top figure) and upward (bottom figure) flow at a wall normal location unwrapped at $2r/D$=0.95 (y^+=5.5)

[1] At: https://www.ike.uni-stuttgart.de/forschung/sco2/dns/

DOI: 10.17185/duepublico/48873

In the first *5D* section, streaks start stretching close to the wall and this elongation later spreads to the bulk region. Moreover, the intensity of the streaks decreases significantly. The low-speed streaks disappear from the flow in the deteriorated heat transfer regime (z=10D-22D). Additionally, the high-speed streaks elongate, particularly in the streamwise direction indicating 'rod-like'-turbulence structures in the near-wall area for deteriorated heat transfer. The high-speed streaks become intense in their magnitude and ultimately start breaking down into smaller scales. The low speed streaks reappear after z=*22D* and hinder the further growth of the high-speed streaks. Both high and low speed streaks are present in the recovery zone in the near-wall region.

Fig. 6 shows the iso-surfaces of low and high speed streaks along with the iso-surface of a vortex criterion (sometimes denoted as λ_2) to visualize these and other coherent turbulent structures. It starts reducing in the downstream direction and shifts away from the wall. The low-speed streaks are suppressed and the intensity of the coherent structure is reduced significantly. Moreover, high-speed streaks survive in the flow of the deteriorated heat transfer regime and are stretched in the streamwise direction in the near-wall region as observed earlier. After the reappearance of additional low-speed streaks at z=*15D*, the λ_2 vortex also starts increasing and interestingly the coherent structures are superimposed mainly on the high-speed streaks as highlighted with black circles.

Contrary to downward flow, the upward flow does not exhibit the elongated streaks in streamwise direction. Here, both low and high speed streaks remain in the flow throughout the pipe at all three depicted locations (refer **fig. 7**). Due to buoyancy and deceleration effects, the intensity of these streaks also increases in the streamwise direction. These streaks also widen in the circumferential direction as compared to downward flow. Both low and high streaks are more intense in the upward flow.

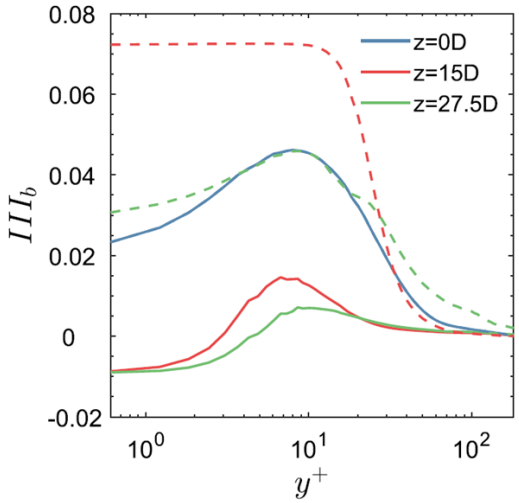

Figure 8: Radial distribution of III_b; solid lines: upward flow and dashed line: downward flow

Figure 8 shows the third invariant of Reynolds stress anisotropy tensor (III_b=$b_{ij}b_{jk}b_{ki}$/3, where b_{ij} is the Reynolds stress anisotropy tensor). It carries information about the nature of the anisotropy. In [10] we have presented it along the wall-normal direction at different streamwise locations in the 'Lumley-Trirangle'. The third invariant has a negative value for the disk like structure (oblate structure) of turbulence and a positive value when the turbulence has the rod-like structure (prolate structure). In case of upward flow, third invariant becomes negative close to the wall and it indicates that turbulence structure is becoming disk-like in which only two principal stresses have significant magnitudes. Due to this disk-like feature, all turbulence structures are stretched in two directions and squeezed in the third direction. As expected, the downward flow has a completely different turbulence close to the wall compared to the upward flow. At z = *15D*, the third invariant has a positive value which indicates, that turbulence became rod-like, i.e., elongated in one direction only. A transition back to the normal state can be seen at z = *27.5D* where the turbulence recovery was observed. The turbulent state remains anisotropic in the near-wall region, while only at the center of the pipe, turbulence becomes isotropic. This explains why the flow is difficult to model.

3.2 WALL QUANTITIES

In **figs. 9 and 10** the wall temperature of simulations with G = 53.8 kg/m^{2}s and q_w=30.87 W/m^2 (denoted as low heat flux) or q_w=61.74 kg/m^{2}s (denoted as high heat flux) are presented for both upward and downward flow in the cooler range of the bulk enthalpie

$$h_b = h_{in} - \frac{q_w}{G}\frac{z}{D} \quad , \qquad (2)$$

where h_{in} is the enthalpy at the inlet position z=*0*, where the cooling begins. The bulk enthalpy represents at any axial position z the energy content in a flow.

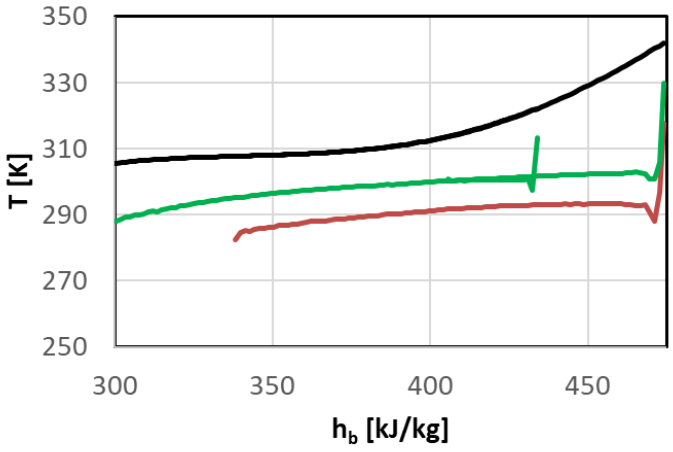

Figure 9: Upward flow with G = 53.87 kg/m^{2}s. Bulk temperature (black) and wall temperature for low (green) and high wall heat flux (brown) vs. the enthalpy h.

DOI: 10.17185/duepublico/48873

For the low heat flux two simulations with different inlet temperatures 342 K~69°C and 322 K are presented, producing an overlap region, where the flow is not fully developed.

The heat transfer is enhanced by buoyancy in the upward flow case compared to the downward flow case due to the unstable thermal stratification (light below heavy fluid) and the associated turbulence production. The forced convection, no gravity, case for the same parameters is presented in **fig. 11**.

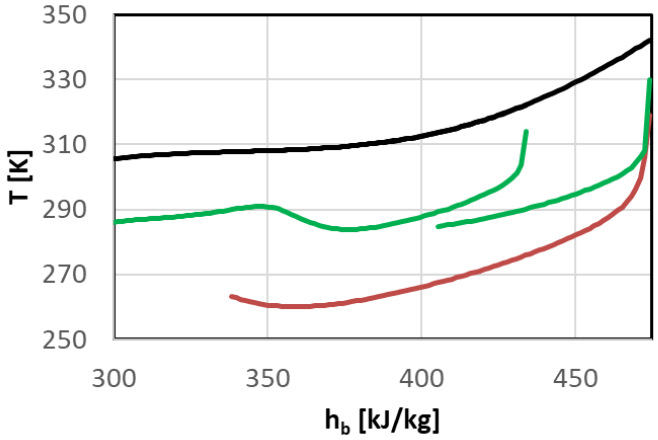

Figure 10: Same as the previous figure for downward flow.

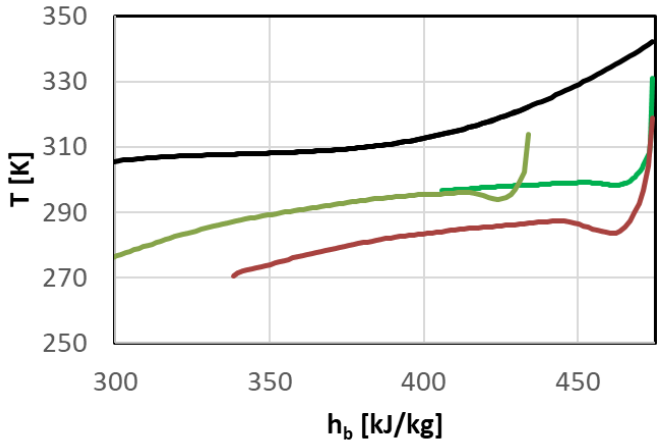

Figure 11: Same as the previous figure for the case without gravity (forced convection case).

This can be explained by the increased (liquid-like) viscosity near the wall when the larger heating is applied.

As a DNS result not only the wall temperature but also the wall shear stress is obtained, presented in fig. 12 for the forced convection case. It is interesting that for the high heat flux case the wall shear stress is larger that for the small heat flux case.

The no-gravity case does not exist physically at this mass flux. However, for the purpose of extrapolation to higher mass fluxes it becomes relevant, see below. The small kink at the end of the DNS domain, also observed in fig. 9, is due to a low-range upstream influence of the imperfect constant-pressure outflow boundary condition.

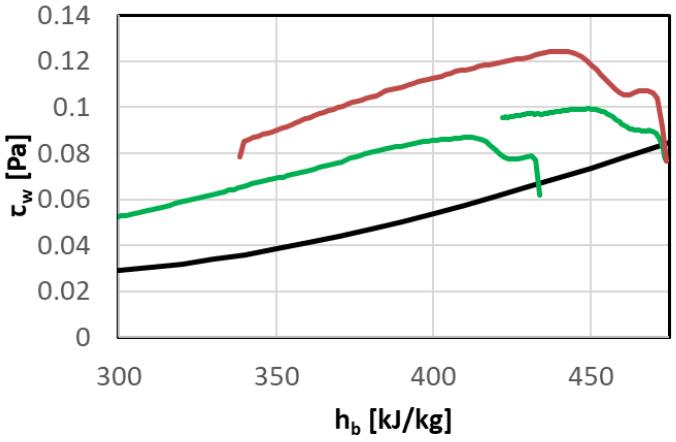

Figure 12: The wall shear stress for forced convection flow with G = 53.87 kg/m^{2}s. For low (green) and high wall heat flux (brown) vs. the enthalpy h. The constant-property value is shown for comparison (black).

3.3 POLYNOMIAL APPROXIMATION

In order to make our DNS results applicable to engineering analysis, we have approximated their wall temperature by least-squares polynomial fits, see **figs. 13-15**. Strictly, a functional fit is only meaningful, if the flow can be treated locally, or in other words, regarded as 'fully developed'. As this is not the case under some conditions, we have to make this assumption as an approximation! All regions in which we subjectively have classified the flow as non-fully developed have therefore be removed 'by hand' from our data befour the polynomial fit was made. This leaves some gaps in the data, which where bridged by the polynomials.

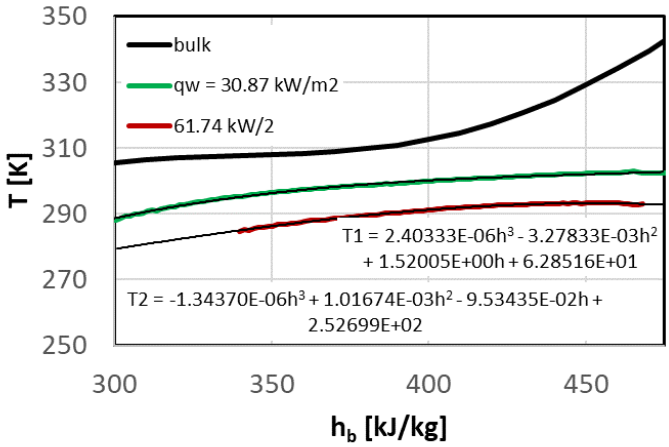

Figure 13: Polynomial fits of the wall temperature, upward flow.

DOI: 10.17185/duepublico/48873

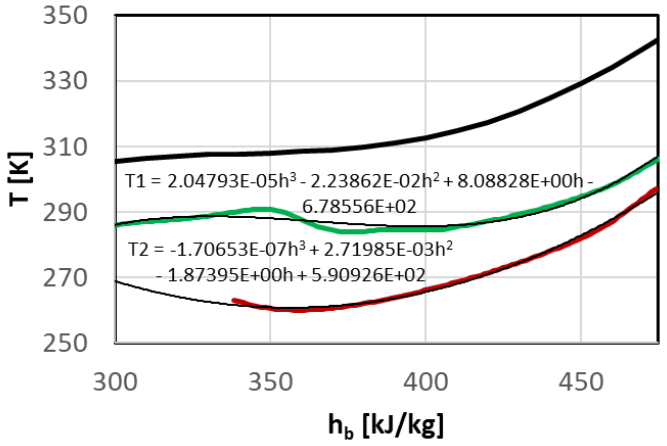

Figure 14: Same as the previous figure for downward flow.

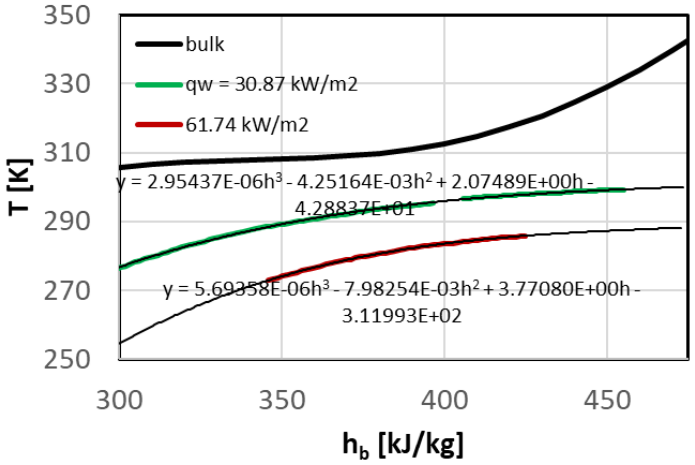

Figure 15: Same as the previous figure for flow without gravity influence (forced flow).

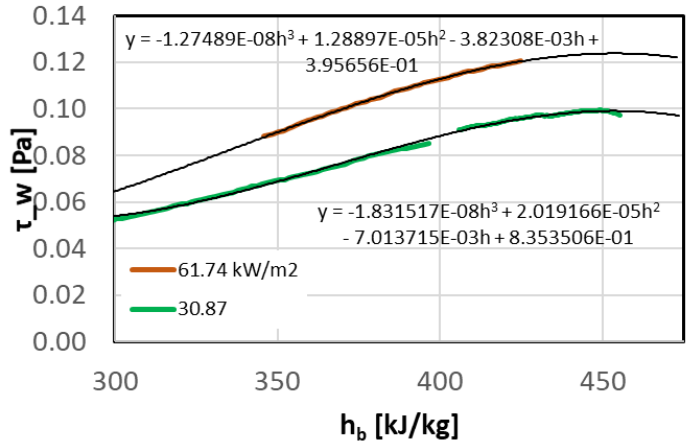

Figure 16: Polynomial fits of wall shear stress for forced flow.

At each enthalpy station, three values of the wall temperature are available: The bulk temperature corresponding to no wall heating, and two temperatures for the two heating rates. From these data the wall heat flux for any given wall temperature can be obtained by piecewise linear interpolation. Extrapolation should be avoided.

In order to demonstrate, that this method is also feasible for the wall shear stress, we present the curve fits of **fig. 16** for the forced convection case. As the third data point the constant-property value of the wall shear stress can be used. However, in this paper the wall shear stress is not investigated further.

The range of validity of our method is:

- pipe diameter is 2 mm
- pressure is close to 80 bars
- mass flux density is $G = 53.78$ kg/m^{2}s
- enthalpy is in the range between 300 and 480 kJ/kg

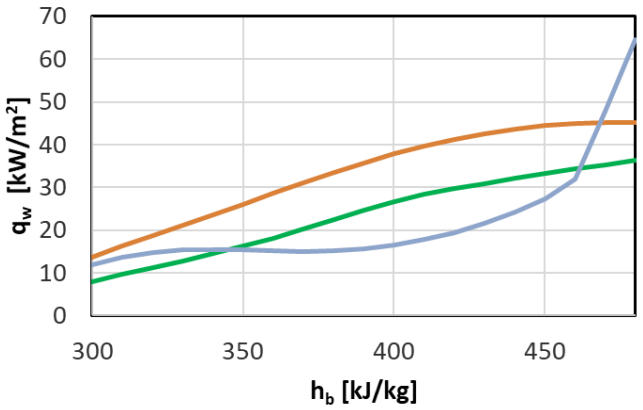

Figure 17: Wall heat flux obtained with our interpolation method at $G = 53.78$ kg/m^{2}s for an assumed wall temperature of 25°C, red: upward, blue: downward, green: forced flow

Next, this interpolation method is used for some practical calculations related to the cooler. Let us make the approximation, that the wall temperature of the (primary) sCO_2-side of the cooler is $T_W = 25$°C. We may regard our investigation as a limiting case, because this can in practice be achieved only approximately by a high mass flux of the secondary side with a fluid (e.g. water) of that temperature. With this assumption, the wall heat flux of a representative channel of the cooler can be determined by our interpolation method as a function of the enthalpy, see **fig. 17**.

From the figure it becomes obvious that the upward flow is favorable because leads to the highest heat flux over almost the entire enthalpy range due to buoyancy production of turbulence. However, this result has little practical value, because in practice the mass flux G will be much higher (up to 2000 kg/m^{2}s) and the influence of buoyancy may disappear with higher mass flux.

4.1 SCALING TO HIGHER MASS FLUX

We can expect that the effect of buoyancy decreases with higher mass flux. Therefore, the question must be investigated next, for which mass flux buoyancy can be neglected.

DOI: 10.17185/duepublico/48873

A buoyancy parameter

$$Bo^* = \frac{Gr^*}{\mathrm{Re}^{3.425}\,\mathrm{Pr}^{0.8}} \qquad (3)$$

has been defined in [13] for gases on the basis of the Reynolds- und Grashof numbers

$$\mathrm{Re} = \frac{GD}{\mu_b} \quad ; \quad Gr^* = \frac{g\beta_b\,\rho_b^2\,q_w D^4}{\lambda_b \mu_b^2} \quad . \qquad (4)$$

This parameter can be used as an indicator to determine whether buoyancy has an effect: buoyancy can be neglected if it is smaller than 10^{-6} [13]. This applies for our cooler channel cases with G > 500 kg/m²s as shown in **fig. 18**. In the other cases buoyancy should be considered. With this information it becomes clear that the forced convection case is important for further consideration.

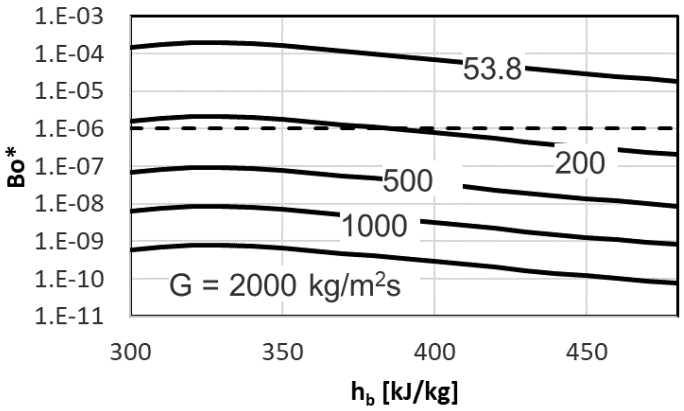

Figure 18: Buoyancy parameter Bo^* as a function of the bulk enthalpy for various mass-flux densities G under the assumption of T_w = 25°C, - - - - limiting value.

4.2 COMPARISON TO EMPIRICAL CORRELATIONS

In the following we will assume, that buoyancy has no effect. The heat transfer of such forced convection has been approximated with various empirical correlations given in [3], which are compared for G = 53.78 kg/m²s in **fig. 19** with our forced convection case. None of the existing correlation agrees exactly with our DNS results but a recommendation, which correlation can be used for practical calculations is given as follows:

- Bringer and Smith gives good prediction for a low enthalpy range but underestimate it if h > 350 kJ/kg,
- Pitla et al. overestimate the heat flux drastically, in the region h > 400,
- Krasnochekov et al. and Baskov et al. overestimate the heat flux drastically,
- Jackson's as well as Mokry-Poiro's correlation have been developed for wall heating but for cooling they underestimated the heat flux only slightly. They can be recommended for further use.

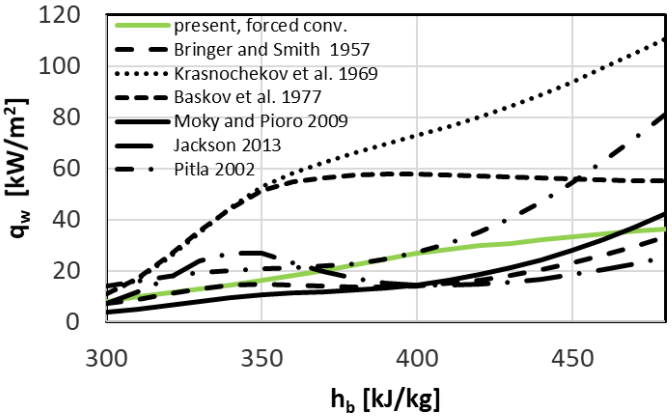

Figure 19: Wall heat flux at G = 53.78 kg/m²K for various correlations and our DNS results for forced convection (green).

4.3 SCALING TO HIGHER MASS FLUX

A DNS for higher mass flux cannot be performed due to the extremely high numerical effort, that would be necessary. Therefore, we make an attempt to develop a scaling method. **Table 1** presents a list of the exponents used in the Nusselt correlations of the form

$$\mathrm{Nu}_b = \frac{q_w\,D}{(T_b - T_w)\,\lambda_b} = C\,\mathrm{Re}_b^n\,\mathrm{Pr}_b^m \left(\frac{\rho_b}{\rho_w}\right)^p \left(\frac{\mu_b}{\mu_w}\right)^s \quad . \qquad (5)$$

If the mass flux density G changes only the Reynolds number will change and all other quantities remain constant due to our assumption of a constant wall temperature. **Table 1** gives an overview of n used by the correlations given in [3]. Values are in the range 0.55 < n < 0.82.

A scaling method relates two mass fluxes G_1 and G_2 to the two corresponding heat fluxes q_{w1} and q_{w2} using a power law with the exponent n

$$\frac{q_{w2}}{q_{w1}} = \left(\frac{G_2}{G_1}\right)^n \quad . \qquad (6)$$

Table 1: The exponent n in the correlations given in [3]

Authors	year	*n*
Bringer & Smith	1957	0.77
Yoon et al.	2003	0.69
Son and Park	2006	0.55
Oh and Son	2010	0.7
Jackson	2002	0.82
Huai and Koyama	2007	0.8
Lee et al.	2013	0.56
Saltanov	2015	0.823
Simoes et al.	2008	0.8

DOI: 10.17185/duepublico/48873

As case 1 the above presented simulation case with G = 53.78 kg/m^{2}s is used. Case 2 is a case with an arbitrary higher heat and mass flux. No theoretical, value of n exists. In the following we use n = 0.55 and n = 0.8 in order to provide some guidelines. The same deviations as above are observed for high mass flux G = 1000 kg/m^{2}s, **fig. 20**.

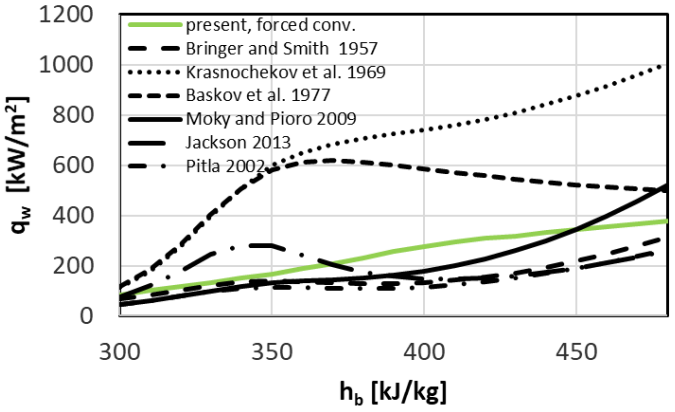

Figure 20: Wall heat flux at G = 1000 kg/m^{2}s (right), for various correlations and our DNS results, scaled with n = 0.8, for forced convection (green).

4.4 MINIMUM LENGTH OF THE COOLER

The minimum length L of the heat exchanger, which is at least necessary to the transfer the heat necessary to cool the CO_2 to the desired outlet temperature, is

$$L = \frac{G \cdot D}{4} \int_{h_{in}}^{h_{out}} \frac{1}{q_w} dh \quad . \tag{7}$$

Numerical values are presented in **fig. 21** calculated with various correlations and the present method as a function of G. Again, large deviations between the results appear.

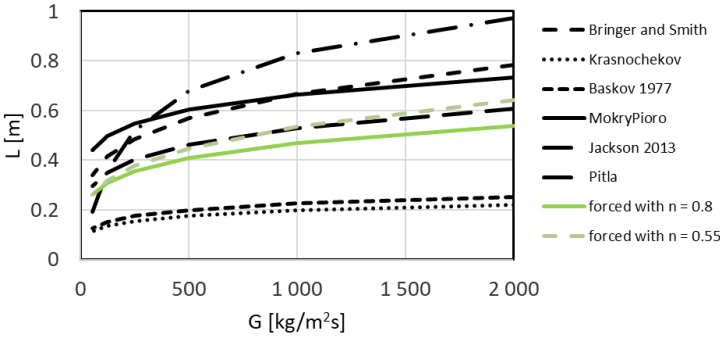

Figure 21: Minimum length L of the cooler calculated with correlations and our forced case with n = 0.8 and n = 0.55.

5. CONCLUSIONS

Direct numerical simulations have been performed to investigate the flow and heat transfer of supercritical CO_2 within representative channels of the cooler (condenser) of a proposed Brayton Cycle. The wall-temperature obtained from DNS for two cases with different wall heat fluxes are smoothed and fitted with a 3rd-order polynomials to constitute a practical prediction method for the wall heat flux at any given wall temperature based on interpolation. It is also found, that predictions of the minimum cooler length using the various methods differ by up to a factor of two! None of the existing correlation agrees completely with our DNS results but a recommendation, which correlation can be used for practical calculations is given.

NOMENCLATURE

C	-	constant in a correlation
c_p	kJ/kgK	specific heat capacity
g	m/s^2	gravity acceleration
G	kg/m^2s	mass flow density
Gr	-	Grashof number
D	m	pipe diameter
h	kJ/kg	specific enthalpy
L	m	minimum length of the cooler
n	-	exponent of Re in a correlation
Nu	-	Nusselt number
m	-	exponent in a correlation
p	Pa	pressure
Pr	-	Prandtl number
q_w	kW/m^2	wall heat flux
Re	-	Reynolds number
s	-	exponent in a correlation
t	s	time
T	K	temperature
u_i	m/s	velocity component
β	$1/K$	thermal expansion coefficient
λ	W/mK	heat conductivity
μ	$Pa\,s$	dynamic viscosity
ρ	kg/m^3	density
τ_w	Pa	wall shear stress

Indices

ax	axial direction
b	bulk
in	inlet
pc	pseudo critical
w	wall

DOI: 10.17185/duepublico/48873

ACKNOWLEDGEMENTS

This work has been supported by the *Forschungsinstitut für Kerntechnik und Energiewandlung e.V., Stuttgart* and the *High-Performance Computer Center (HLRS) Stuttgart*.

REFERENCES

[1] V. Dostal, M. Driscoll, and P.A. Hejzlar: Supercritical carbon dioxide cycle for next generation nuclear reactors, Tech. rep. MIT, 2004

[2] E. Lemmon, M. Huber, and M. McLinden: NIST standard reference database 23: reference fluid thermodynamic and transport properties-REFPROP, version 9.1, 2013

[3] L. F. Cabeza, A. de Garcia, A.I. Fernandez, and M.M. Farid: Supercritical CO_2 as heat transfer fluid: A review, Applied Thermal Engineering 125 (2017), 799-810

[4] K. Brun, P. Friedman, and R. Dennis: Fundamentals and Applications of Supercritical Carbon Dioxide (sCO_2) Based Power Cycles, Elsevier, Cambridge, MA (2017)

[5] J.H. Bae, J.Y. Yoo, and H. Choi: Direct numerical simulation of turbulent supercritical flows with heat transfer, Phys. Fluids 17 (10) (2005).

[6] X. Chu, and E. Laurien, Direct numerical simulation of heated turbulent pipe flow at supercritical pressure, J. Nucl. Eng. Radiat. Sci. 2 (2016)

[7] H. Nemati, A. Patel, B.J. Boersma, and R. Pecnik: Mean statistics of a heated turbulent pipe flow at supercritical pressure, Int. J. Heat Mass Transfer 83 (2015) 741–752

[8] S. Pandey, X. Chu, and E. Laurien, and B. Weigand: On the Effect of Non-Uniform Body Force on Turbulence in a Channel Flow, under review.

[9] S. Pandey, X. Chu and E. Laurien: Investigation of in-tube cooling of carbon dioxide at supercritical pressure by means of direct numerical simulation, Int. Journal of Heat and Mass Transfer 114, 944 – 957 (2017)

[10] S. Pandey, E. Laurien, and X. Chu: Flow and Heat Transfer Characterization for Supercritical CO_2 During Heat Rejection, 2nd European CO_2 Conference, Essen, Germany, Aug. 30-31, 2018

[11] S. Pandey, E. Laurien, and X. Chu: Development of direct numerical simulation database for supercritical carbon dioxide, 6th International Supercritical CO_2 Power Cycles Symposium, Pittsburgh, PA, March 27 - 29, 2018

[12] S. Pandey, X. Chu, E. Laurien and B. Weigand: Turbulence modulation during heat rejection by a fluid at supercritical pressure, Physics of Fluids 30, 065105 (2018)

[13] D.M. McEligot and J.D. Jackson: 'Deterioration' criteria for convective heat transfer in gas flow through non-circular ducts, Nuclear Engineering and Design 232 (2004), 327-333

DOI: 10.17185/duepublico/48873

DOI: 10.17185/duepublico/48873
URN: urn:nbn:de:hbz:464-20190927-132213-9